CHAPTER V

DEPENDENCE OF LOW-FREQUENCY VARIABILITY ON GALACTIC COORDINATES

5.1 INTRODUCTION

A reliable signature of any propagation effect is its dependence on the effective path-length through the medium responsible for it. For extragalactic objects, the path-length through the interstellar medium (ISM) is a function of galactic latitude and longitude (irrespective of the details of the assumed model for the ISM). Hence, if low-frequency variability (LFV) is due to refractive interstellar scintillation (RISS), it is expected to show some functional relationship with galactic latitude and longitude. The presence of such an effect was first claimed by Cawthorne and Rickett (1985) who used the results of the Bologna monitoring programme (Fanti et al., 1981) to show that the mean galactic latitude of those sources with variability time-scales of a few months was significantly smaller than that of the nonvariable sources. From the same data, Spangler et al. (1987) also have shown a latitude dependence for the 'short-term' variability (with time-scales of a few months to a couple of years). The related phenomenon of cm-wavelength flickering has also been found to possess a galactic-latitude dependence (Heeschen and Rickett, 1987), although there has been a recent report of the nondetection of any such effects by Dennison and Cordes (1990).

A short-coming of almost all previous low-frequency flux-density monitoring programmes has been that sources whose lines-of-sight have long path-lengths through the disk of the Galaxy ($|b| < 10°$) have been excluded. In view of this, we selected a sample of 96 compact flat-spectrum sources, evenly distributed over all latitudes, with which to study the latitude dependence of LFV. Special attention was given to investigating any significant differences in the low-frequency-variability properties of sources seen in the direction of the galactic centre and those lying towards the anticentre. If LFV is due to RISS, the predicted time-scales of flux-density variations at 327 MHz would be of the order of 100 yr for sources seen through the centre of the Galaxy. In contrast, the corresponding time-scales predicted for high-latitude sources are only a few months. As a compromise, we decided to study the flux-density variations of sources at all latitudes over a time interval of about 15 yr. This was accomplished by comparing our measurements made during 1986-1987 with flux densities extrapolated to 327 MHz (using published spectral information) from the 408-MHz measurements made with the Molonglo Cross during 1969-1975 for high and intermediate-latitude sources ($|b| > 3°$) and 1969-1971 for low-latitude ($|b| < 3°$) sources (Large et al., 1981; Clark and Crawford, 1974).

In this chapter, we describe the observations and the latitude dependence of LFV derived from this study. The results are then compared with semi-quantitative predictions from the theory of RISS for the galactic-coordinate dependence of LFV assuming a number of plausible distributions for the turbulent ionized component of the interstellar medium.

5.2 THE SAMPLE

The aim of the experiment was to detect flux-density variations at 327 MHz for a sample of flat-spectrum sources over a time interval of about 15 yr. Since the flux densities at the first epoch are estimated from 408-MHz measurements with the Molonglo Cross, all the sources chosen are from two Molonglo source catalogues. These are:

(a) The Molonglo Reference Catalogue of Radio Sources (Large et al., 1981) covering the whole sky south of declination +18° and at galactic latitudes $|b| > 3°$. The survey observations were made during 1969-1975 and it is complete for $S_{408} > 1.0$ Jy. Multiple observations were made for a majority of sources, and position and flux-density values averaged for these cases.

(b) The Molonglo Low-Latitude Survey (Clark and Crawford, 1974) covering the region $|b| < 3°$ and declinations < +18°. These observations were made during 1969-1971. The catalogue goes down to $S_{408} = 0.6$ Jy but is not complete because of confusion in the galactic plane. These observations were made between 1969 and 1971.

The chosen sample is distributed over all galactic latitudes and longitudes observable with the OSRT, and consists of 96 sources (Table V-1) from these two catalogues selected on the following criteria:

(i) The declinations of the sources lie in the range $-36° \leq \delta \leq +18°$. The northern cut-off is set by the northern limit of the Molonglo survey, while the southern limit is set by the declination range over which Ooty observations are sensitive.

(ii) The spectral indices of the sources, α, (defined as $S_\nu \propto \nu^{-\alpha}$) are

less than +0.5 between 408 MHz and 5 GHz. This condition was included since most low-frequency variable sources have flat spectra (Condon et al., 1979). For high-latitude sources ($|b|>10^{\circ}$), spectra were taken from the compendium of Kuhr et al. (1981a, b), VLA observations by Perley (1982) and the VLA calibrator list. The Molonglo flux densities have been converted from the flux-density scale of Wyllie (1969) to that of Baars et al. (1977), which was also used for calibration of our measurements. For the lower-latitude sources, spectra were estimated using the following observations:

(a) The stronger sources from Clark and Crawford ($|b| < 3^{\circ}$) have been observed at 5 GHz by Caswell and Clark (197).

(b) A sample of low-latitude sources ($|b| < 10^{\circ}$) with compact components (based on interplanetary-scintillation measurements) has been observed at 1.4, 5 and 15 GHz with the VLA (Rao et al., 1990). A few of our sources are contained in this sample.

(c) Additional information on the spectra are from Dennison et al. (1984).

(iii) Sources should show evidence for the presence of a compact component either from Very Long Baseline Interferometry (VLBI) or from 15-GHz observations made with the VLA in its A configuration. To some extent, this condition overlaps with (ii) but was included since, in all models of low-frequency variability, only very compact components are predicted to show LFV. We have tried explicitly to confirm that all the sources in Table V-1 contain milliarcsecond structures and are thus potential metre-wavelength variables. For sources marked I in column 6 of Table V-1 there are VLBI observations at 2.29 GHz, showing the existence of

significant flux density at a baseline of 8×10^7 λ, corresponding to an angular size of ~ 3 mas (Morabito et al., 198). VLBI observations of some of the low-latitude sources using the European VLBI Network (EVN) at λ 6 and 18 cm led us to detect milliarcsec components in them. These sources are marked as II in Table V-1. In Chapter VI, we present these observations in detail. For sources marked III, 15-GHz observations with the VLA in its A configuration show that the measured visibility at the longest baseline decreases only by < 10% from its maximum value, indicating angular sizes of less than 50 mas (VLA calibrator list, Rao et al., 1990). For sources marked IV, interplanetary-scintillation observations at metre wavelengths show the existence of components with angular sizes of < 200 mas at metre wavelengths (Rao and 1988). The sources for which no mas-structural information could be found are marked as V.

(iv) The expected flux densities of the sources at 327 MHz should $\geq$ 1 Jy for ease of measurement (Chapter III).

All 96 sources are listed in Table V-1.

Control sources:

We also selected a sample of 14 steep-spectrum double sources. These are not expected to show variations and so form a control sample to check the accuracy of our methods of observation and analysis. Spectra and structures for these sources were obtained from the MIT-Green Bank survey (Bennett et al. 1986 and Lawrence et al. 1986). All the control sources have spectral indices $\alpha > +0.5$, are in the Molonglo Catalogue with 408-MHz flux densities $\geq$ 1 Jy and are doubles with component separations between 8 and 15 arcsec. Larger sources were not considered as these

would have been resolved by the OSRT. Table V-2 lists these sources.

Calibrators:

24 calibration sources spanning all right-ascensions and the declination range of the OSRT, and selected from the standard OSRT calibrator list, were also included in the programme. These sources are listed in Table V-3.

5.3 FLUX DENSITIES AT THE FIRST EPOCH :

For all sources, we gathered spectral information from the various catalogues and estimated their spectral indices below 1 GHz. These were used to extrapolate from the Molonglo measurements at 408 MHz and estimate the first-epoch flux densities at 327 MHz. Flat-spectrum compact sources are generally variable at centimetre wavelengths, leading to errors in determining spectra when the measurements for different frequencies are made at different times. Unfortunately, this is usually the case. However, the resulting flux-density error at 327 MHz is small since the frequency difference between 408 and 327 MHz is itself small. The uncertainty in the extrapolated flux densities at 327 MHz can be calculated by,

$$\left(\frac{\Delta S_{327}}{S_{327}}\right)^2 = \left(\frac{\Delta S_{408}}{S_{408}}\right)^2 + \left(\ln(408/327)\ \Delta\alpha\right)^2$$

$$= \left(\frac{\Delta S_{408}}{S_{408}}\right)^2 + \left(0.2\ \Delta\alpha\right)^2 \qquad \text{------(5.3.1)}$$

The error in Molonglo-Reference-Catalogue measurements at 408 MHz is typically 5% and, since our estimates of the spectral indices are correct to about 0.2, we believe that the uncertainities of the estimated flux densities at 327 MHz are about 7% for the high-latitude sources, but 10%

for sources with $|b| < 3°$, which have larger errors in the measured flux densities at 408 MHz. The estimated 327-MHz flux densities for the compact sources, control sources and calibrators at the first epoch are given in Tables V-1, 2 and 3 respectively.

5.4 THE OOTY OBSERVATIONS

The second-epoch observations were made using the method described in Chapter III. For the low-latitude sources, an additional correction factor had to be included for the increase in the sky-background temperature which at 327 MHz is comparable to the receiver temperature for the ORT. This was needed because the automatic level-controller circuit (ALC) at the input to the sampler (Section 3.3) holds the quantity $|g|^2(T_r + T_a)\,\Delta\nu$ (where, T_r is the receiver temperature and T_a is the antenna temperature) constant by adjusting the voltage gain factor, g of the system. Hence, for sources in the galactic plane, the estimated gain factors from the observed correlated flux densities of calibration sources situated in 'cold' regions of the sky need scaling by a factor,

$$F_s = \sqrt{(T_{s2}/T_{s1})} \qquad \text{------(5.4.1)}$$

where, T_{s2} = the system temperature in the galactic plane

and T_{s1} = the system temperature with the telescope pointing to a calibration source.

This effect is important only for the ORT sections since the collecting area of the baby-cylinders is so small that the effective system tenperature does not change significantly with coordinate. We have measured the increase in the power level (ΔP) at the input to the sampler by bypassing the ALC temporarily for one of the ORT sections, OE, and observing all the sources in our sample seen at low latitudes in the galactic-centre quadrant. We have found appreciable changes in the power

level ($\Delta P \geq 0.1$dB) for three sources. Table V-4 lists these sources and the corresponding correction factor in each case, which was calculated as follows:

$$F_s(OE) = \sqrt{(T_{s2}/T_{s1})}$$

$$= 10^{\Delta P/20}$$ where, ΔP is the change in the power level in dB

which can be written as:

$$= \exp\left(\frac{\Delta P \ \ell n\ 10}{20}\right) \qquad \text{------(5.4.2)}$$

For any other ORT-section (OX):

$$F_s(OX) = \exp\left(\frac{\Delta P \ \ell n\ 10}{20}\right) * (g_{OE}/g_{OX}) \qquad \text{------(5.4.3)}$$

where, g_{OE} and g_{OX} are the voltage gain factors determined from the observations of the calibration sources.

5.5 RESULTS

Table V-1 presents both the first-epoch flux densities and the results of the Ooty observations. The different columns are arranged as follows:

Column 1 : Source name

Column 2,3 : Galactic longitude and latitude.

Column 4 : Spectral index, α ($S_\nu \propto \nu^{-\alpha}$) between 408 MHz and 5 GHz.

Column 5 : Reference for flux density at 5 GHz.

Column 6,7 : Classification according to the presence of milliarcsec components and references (as detailed in section 5.2).

Column 8,9 : Estimated first-epoch flux density at 327 MHz and error.

Column 10,11: Measured second-epoch flux density and error.

Column 12 : Variability index, defined as:

TABLE V-1: TWO EPOCH FLUX-DENSITY MEASUREMENTS OF THE COMPACT-SOURCE SAMPLE

NAME	l	b	α(5,408)	REF[a]	VLBI CL.	REF[b]	$S_{327}(72)$	ERR	$S_{327}(86)$	ERR	V(%)	VAR
0003-066	94	-66.6	0.21	K	I	1	2.10	0.09	1.94	0.07	-7.7	
0013-005	104	-61.8	0.14	K	I	2	1.00	0.10	1.17	0.05	16.8	Y
0019-000	108	-61.8	0.35	K	I	7	2.35	0.07	2.56	0.05	8.7	
0048-097	122	-72.4	-0.34	K	I	1,3	0.80	0.06	1.04	0.10	29.4	Y
0112-017	137	-63.7	-0.11	K	I	1,2	0.75	0.09	0.70	0.06	-6.3	
0118-272	214	-83.5	0.18	K	I	1	1.42	0.06	0.90	0.07	-36.4	Y
0146+056	148	-54.1	-0.03	P	I	1,2	0.75	0.06	0.64	0.05	-15.1	Y
0202+149	148	-44.0	0.16	P	I	1,2,5	5.25	0.25	5.12	0.13	-2.5	
0202-172	186	-70.2	-0.07	P	I	1	1.05	0.05	1.29	0.07	23.0	Y
0221+067	160	-49.1	0.27	P	I	1,2	1.50	0.05	1.24	0.08	-17.0	Y
0229+131	157	-42.7	-0.03	P	I	1,2	2.15	0.11	1.95	0.12	-9.4	
0235+164	157	-39.1	-0.25	P	I	1,2,3	1.00	0.06	1.14	0.06	14.0	
0237+040	167	-49.1	0.14	P	I	1	0.98	0.09	0.71	0.05	-27.3	Y
0237-233	210	-65.1	0.04	P	I	1	2.10	0.11	3.00	0.16	43.0	Y
0336-019	188	-42.5	-0.15	P	III		1.92	0.07	1.39	0.15	-27.8	Y
0403-132	206	-42.7	0.39	K	I	1	6.80	0.06	6.49	0.19	-4.6	
0420-014	195	-33.1	-0.34	P	III		1.55	0.10	1.19	0.06	-23.4	Y
0430+052	190	-27.4	0.21	P	I	10	6.50	0.19	4.28	0.23	-34.1	Y
0451-282	229	-37.0	0.05	P	I	1	2.45	0.11	2.65	0.28	8.2	
0529+075	197	-13.7	0.07	P	III		2.10	0.08	2.10	0.14	0.0	
0538+133	193	-8.9	0.42	OH	IV		1.41	0.04	1.07	0.08	-23.9	Y
0554+130	195	-5.7	0.46	OH	III	8	1.62	0.07	1.61	0.08	-0.9	
0605-085	216	-13.5	-0.03	P	I	5	2.55	0.11	3.01	0.16	18.1	Y
0607-157	223	-16.2	0.57	P	I	5	2.70	0.36	0.95	0.07	-64.8	Y
0611+131	197	-2.2	0.50	D	II	9	0.97	0.05	1.08	0.07	11.6	

0629+104	202	0.5	0.49	C	II	9	3.20	0.05	2.92	0.18	-8.9	
0648-165	228	-7.7	-0.11	P	II	9	2.00	0.06	1.99	0.10	-0.3	
0650-063	219	-2.6	0.20	D	II	9	0.80	0.09	0.71	0.06	-10.9	
0700-007	215	2.3	0.30	D	II	9	1.00	0.04	1.01	0.07	0.7	
0705-142	228	-2.9	0.30	D	II	9	0.66	0.08	0.73	0.06	10.8	
0719+056	211	9.2	0.43	OH	IV		1.36	0.07	1.40	0.09	2.7	
0723-008	218	7.2	0.09	P	I	1	2.95	0.13	3.05	0.21	3.4	
0727-115	228	3.1	0.00	P	I	1	2.65	0.13	1.85	0.10	-30.1	Y
0728-235	238	-2.5	0.40	C	V		1.70	0.07	2.26	0.12	33.0	Y
0733-174	234	1.4	-0.20	D	I	1	1.50	0.06	1.34	0.07	-10.7	
0735+178	202	18.1	0.08	D	I	1,2,3	2.40	0.13	1.85	0.11	-22.8	Y
0736+017	217	11.4	0.17	P	I	5	2.15	0.11	1.24	0.07	-42.1	Y
0742+103	210	16.6	-0.40	P	III		1.00	0.08	1.42	0.07	41.6	Y
0748+126	208	18.8	-0.01	P	I	1,2	1.50	0.08	2.96	0.16	97.6	Y
0812-355	253	-0.6	0.50	C	V		1.30	0.05	1.69	0.18	30.1	Y
0839+187	207	32.5	-0.10	P	I	2	0.63	0.04	0.79	0.05	25.2	Y
0859-140	242	20.7	0.24	P	I	1	3.20	0.18	3.85	0.20	20.2	Y
0925-203	252	21.4	0.16	P	I	10	1.45	0.03	1.16	0.06	-20.1	Y
0952+179	217	48.4	0.38	K	I	2	1.75	0.08	1.59	0.05	-9.3	
1020-103	254	37.8	0.55	P	I	3	1.85	0.05	1.47	0.08	-20.4	Y
1117+146	239	65.3	0.43	K	III	11	3.40	0.09	2.54	0.06	-25.4	Y
1148-001	273	58.8	0.25	K	I	1,2	2.95	0.09	3.20	0.09	8.5	
1213-172	291	44.5	0.28	K	I	1	3.00	0.07	2.48	0.09	-17.4	Y
1226+023	290	64.4	0.26	K	I	1,2	62.00	0.10	54.07	1.90	-12.8	
1252+119	306	74.5	0.05	K	I	1,6	0.90	0.04	0.99	0.10	9.8	
1253-055	305	57.1	0.02	K	I	2	17.00	0.09	13.35	0.20	-21.5	Y
1502+106	11	54.6	0.00	P	I	6	1.85	0.07	0.86	0.06	-53.3	Y
1504-166	344	35.1	-0.11	K	I	1,2,5	1.75	0.06	1.16	0.06	-33.8	Y
1510-089	351	40.1	0.00	P	I	2,5	3.45	0.16	2.27	0.12	-34.2	Y
1514-241	341	27.6	-0.13	K	I	1	1.40	0.07	1.99	0.10	41.8	Y

1532+016	7	43.2	0.20	P	I	1	1.20	0.08	1.15	0.06	-4.2	
1538+149	24	48.8	0.14	P	I	1,3	2.50	0.12	2.93	0.15	17.0	Y
1548+056	14	42.2	0.18	P	I	1	2.60	0.17	2.17	0.11	-16.7	Y
1555+001	10	37.7	0.06	P	III	11	1.10	0.05	0.96	0.06	-12.8	
1622-253	352	16.3	0.16	P	I	1,2	2.35	0.08	2.13	0.22	-9.4	
1622-297	349	13.3	0.03	P	I	1,2	2.80	0.10	3.41	0.18	21.8	Y
1730-130	12	10.8	0.09	P	I	5	5.75	0.29	6.03	0.32	4.9	
1741-038	22	13.1	-0.26	P	I	5	1.35	0.08	0.80	0.05	-40.9	Y
1748-253	4	0.6	-0.35	P/A	II	9	0.73	0.09	0.78	0.09	6.7	
1816-029	27	5.8	0.06	A	II	9	0.97	0.08	0.74	0.05	-23.6	Y
1819-096	21	1.9	0.20	D	III	4	11.43	0.20	9.34	0.49	-18.3	Y
1821+107	39	10.9	-0.22	P	II	9	0.73	0.06	0.42	0.10	-42.7	Y
1830-211	12	-5.7	0.12	A	I/II	2,9	10.55	0.50	9.09	0.48	-13.8	
1845+018	34	1.7	0.50	D	II	9	1.00	0.09	1.27	0.07	27.3	Y
1908-201	17	-13.2	-0.11	P	I	1,2	1.85	0.10	1.89	0.10	2.2	
1910+052	40	-2.3	0.40	D	II	9	0.85	0.06	0.82	0.07	-3.9	
1921-293	9	-19.6	-0.24	P	I	1,2	5.35	0.25	7.74	0.82	44.7	Y
2008-068	36	-20.8	0.12	P	I	1	1.65	0.08	0.92	0.05	-44.2	Y
2029+121	56	-15.8	0.27	P	I	1	1.40	0.09	1.05	0.08	-24.7	Y
2037-253	20	-34.2	0.14	P	I	1,2	0.95	0.09	0.83	0.09	-13.0	
2128-123	41	-41.0	-0.26	P	I	1,2	1.50	0.07	1.38	0.07	-8.2	
2131-021	52	-36.5	-0.15	P	I	6	1.80	0.04	1.78	0.09	-1.3	
2134+004	56	-35.6	-0.82	P	I	12	1.25	0.07	0.77	0.08	-38.4	Y
2136+141	69	-27.5	-0.24	P	I	6	0.73	0.06	0.94	0.05	28.8	Y
2145+067	64	-34.1	0.20	P	I	1	3.80	0.19	3.76	0.20	-1.0	
2150+173	74	-27.7	0.16	P	I	1,6	1.15	0.06	0.94	0.06	-18.2	Y
2155-152	41	-48.0	0.24	P	I	1,2,3	1.80	0.09	1.94	0.08	7.7	
2203-188	37	-51.2	0.29	K	I	2	10.50	0.10	8.26	0.20	-21.3	Y
2210+016	64	-42.0	0.50	P	I	1	4.50	0.09	2.80	0.11	-37.7	
2216-038	59	-46.7	0.11	K	I	1,2	1.50	0.08	1.20	0.05	-20.2	Y

2227-088	55	-51.7	-0.25	K	I	1,2	1.15	0.08	0.89	0.04	-22.3	Y
2240-260	28	-61.4	0.17	K	I	1	1.60	0.09	1.60	0.06	-0.3	
2243-123	54	-57.1	-0.20	K	I	2	1.30	0.05	1.16	0.06	-10.8	
2255-282	24	-64.9	-0.24	K	I	1	0.92	0.04	1.01	0.06	9.5	
2318+049	85	-50.9	-0.13	K	I	1,2	0.77	0.05	0.69	0.03	-9.9	
2320+079	89	-48.6	0.36	K	V		1.50	0.07	1.46	0.06	-2.5	
2328+107	93	-47.1	0.07	K	I	1	1.10	0.09	0.77	0.04	-30.0	Y
2344+092	98	-50.1	0.19	K	I	1	2.30	0.06	2.09	0.07	-9.1	
2345-167	66	-71.9	0.05	K	III	11	2.45	0.09	2.24	0.08	-8.5	
2351-154	72	-72.2	0.03	K	I	1	1.18	0.06	1.05	0.03	-10.6	
2354-117	81	-69.8	0.20	K	I	1	2.60	0.09	2.09	0.06	-19.6	Y

N.B.

a) References for 5-GHz flux densities :

P => Perley et al.(1982); K => Kuhr et al.(1981a,b); D => Dennison et al.(1984); C => Caswell and Clark, (1978); A => Rao et al. (1990);

For three sources, 5-GHz flux densities were not available and the 1.4-GHz flux densities from the Ohio catalogue were used in determining the spectral indices. These are denoted by OH in column 5.

b) References for VLBI / VLA observations on the basis of which the classifications in column 6 are made:

(1) Morabito et al. (1982); (2) Wehrle et al. (1984); (3) Weiler et al. (1980); (4) Dennison et al. (1984)
(5) Romney et al. (1984); (6) Zensus et al. (1984); (7) Hodge & Mutel (1984); (8) Rao et al. (1990)
(9) Rao and Ghosh (1990); (10) Jones (1982); (11) VLA Calibrator list; (12) IAU Symp. No. 110, 151,(1984)

TABLE V-2: TWO EPOCH FLUX-DENSITY MEASUREMENTS FOR THE CONTROL SOURCES

NAME	α(MW)*$_1$	structure*$_2$	$S_{327}(72)$	ERR	$S_{327}(86)$	ERR	V(%)
0001+128	0.87	9.2 D	4.50	0.17	4.57	0.24	-1.56
0015+064	0.91	14.9 D	0.80	0.06	0.98	0.05	22.50
0050+176	1.26	8.8 D	2.85	0.11	2.87	0.16	0.70
0220+064	0.82	10.2 D	1.10	0.05	1.11	0.06	0.91
0246+064	0.78	11.4 D	2.50	0.08	2.61	0.14	4.40
0300+100	0.87	13.9 D	0.93	0.06	0.91	0.05	-2.20
0357+035	1.07	12.6 T	1.05	0.05	1.00	0.10	-4.76
0359+055	0.92	14.8 D	2.40	0.10	2.52	0.13	5.00
0422+124	0.75	8.8 T	0.98	0.04	1.04	0.06	6.12
0532+100	0.86	11.4 D	3.10	0.13	3.06	0.16	-1.29
0718+132	0.98	10.4 D	1.65	0.06	1.55	0.08	-6.06
0840+184	0.89	8.1 D	1.45	0.08	1.15	0.06	-20.69
0940+029	0.63	8.3 D	2.85	0.09	3.07	0.16	7.72
0943+123	0.69	15.0 M	1.40	0.07	1.36	0.07	-2.86

*$_1$: α(MW) represents the metre-wavelength spectral index.

*$_2$: In this column D implies a double, T a triple and M a multiple structure where the number preceding it is the largest angular size in arcsec.

TABLE V-3: TWO EPOCH FLUX-DENSITY MEASUREMENTS FOR THE CALIBRATION SOURCES

NAME	α(MW)	RA(1950)	DEC(1950)	$S_{327}(72)$	ERR	$S_{327}(86)$	ERR	V(%)
0017+154	1.05	0 17 49.98	+15 24 14.5	10.50	0.32	9.89	0.52	-5.8
0114-211	0.35	1 14 25.95	-21 7 55.0	11.50	0.23	12.18	0.64	5.9
0134+329	0.50	1 34 49.83	+32 54 20.5	45.50	0.50	49.19	4.63	8.1
0138+136	0.55	1 38 28.48	+13 38 19.3	7.75	0.29	7.86	0.41	1.4
0218-021	0.80	2 18 22.02	- 2 10 34.1	14.00	0.25	13.33	0.70	-4.8
0350-073	1.00	3 50 5.33	- 7 19 55.4	12.50	0.26	11.80	0.62	-5.6
0358+004	0.80	3 58 33.34	+ 0 28 12.3	5.75	0.23	6.36	0.33	10.6
0406-180	0.40	4 6 52.40	-18 5 0.0	5.95	0.18	5.77	0.30	-3.0
0518+165	0.30	5 18 16.58	+16 35 26.0	17.50	0.75	18.68	0.98	6.7
0732+332	0.50	7 32 41.77	+33 13 50.2	6.50	0.20	7.33	0.71	12.7
0741-063	-0.80	7 41 54.70	- 6 22 20.0	10.50	0.32	10.24	0.54	-2.5
0758+143	0.90	7 58 45.04	+14 23 4.3	9.25	0.25	9.41	0.49	1.7
0855+280	0.65	8 55 10.82	+28 2 29.3	7.27	0.09	8.77	0.44	20.6
1019+222	1.05	10 19 9.42	+22 14 39.5	6.53	0.10	7.11	0.36	8.9
1030-340	1.15	10 30 56.30	-34 3 19.0	6.98	0.25	5.76	0.58	-17.5
1345+125	-0.60	13 45 6.17	+12 32 20.3	8.00	0.27	7.38	0.37	-7.8
1416+067	1.06	14 16 38.77	+ 6 42 20.9	29.00	1.01	32.05	1.60	10.5
1419+419	0.60	14 19 6.29	+41 58 30.2	9.00	0.27	8.09	0.81	-10.1
1436-167	0.55	14 36 41.62	-16 46 7.6	6.13	0.12	5.56	0.28	-9.3
1517+204	0.85	15 17 50.60	+20 26 53.5	9.25	0.40	9.41	0.47	1.7
1547+309	0.75	15 47 12.33	+30 56 20.3	5.10	0.08	5.90	0.59	15.7
1643+022	0.75	16 43 11.12	+ 2 17 9.2	6.25	0.24	6.56	0.33	4.9
2252+129	0.75	22 52 34.53	+12 57 33.5	9.00	0.79	9.12	0.46	1.3
2314+038	0.90	23 14 2.25	+ 3 48 55.2	17.50	0.68	17.07	0.85	-2.3

TABLE V-4: GAIN CORRECTION FOR INCREASED T_{sys} IN THE GALACTIC PLANE

SOURCE	ΔP (dBm)	CORRECTION FACTOR
1748-253	1.2	1.49
1819-096	0.6	1.09
1845+018	1.0	1.124

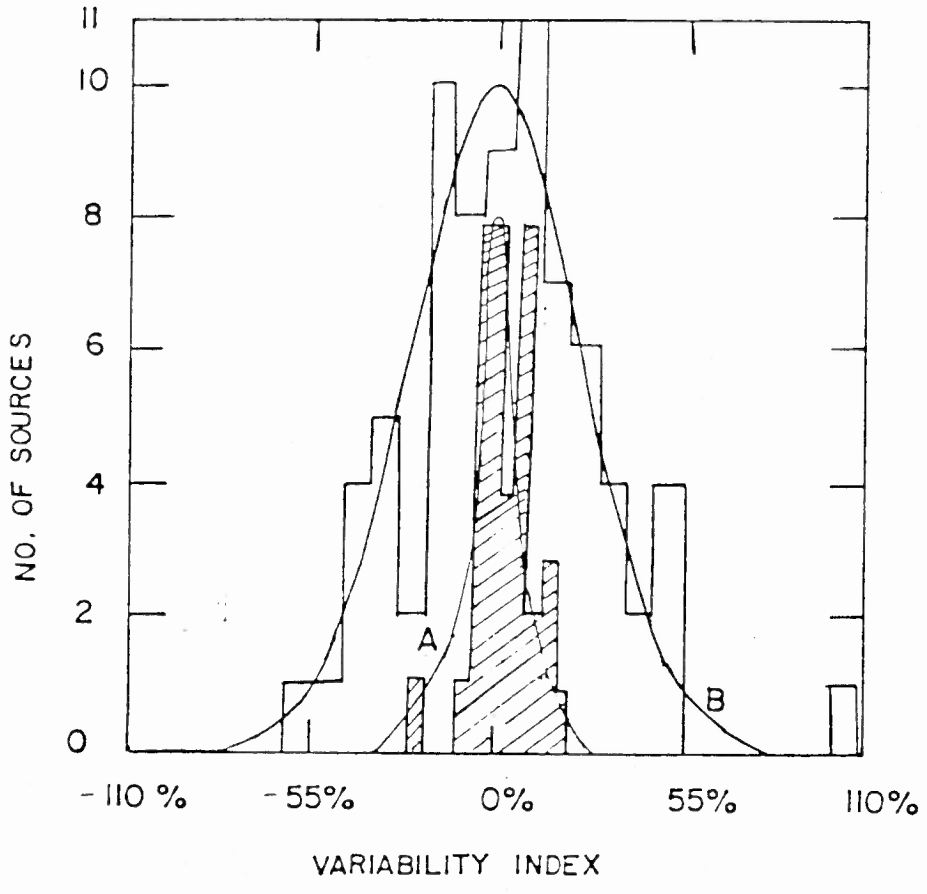

Fig V-1: Histogram of flux density variations for the compact sources (B) and the control sample (A).

$$V = \frac{S\ (\text{epoch } 2) - S\ (\text{epoch } 1)}{S\ (\text{epoch } 1)} \times 100 \qquad \text{------(5.5.1)}$$

Here we have not divided the change in the flux density, ΔS by the mean of S_1 and S_2 since we consider S_1 to be a value closer to the 'true' mean flux-density of the source. This is because the Molonglo survey was made over a period of five years and the majority of catalogued flux-density values are means over several measurements during this period. Also, the spectral indices used to calculate the first-epoch flux density from the Molonglo measurement have been derived using the published flux-density values at various frequencies which were made at different epochs and hence approximate to mean values.

However, the Molonglo Galactic-plane survey was made between 1969 and 1971. In view of the long expected time-scales at 408 MHz for RISS at low latitudes, the S_1 value here do not represent a true mean. The correction factor for this which has to be applied when calculating the modulation index is discussed below.

Column 13 : Sources with variability indices of 15 % or more are marked as variables.

In Table V-2 and V-3 we present the two-epoh flux densities for the control and calibrator sources.

Fig. V-1 presents histograms of the variability indices (V) for the control and calibration sources (A), superposed on a similar histogram (B) for the compact sources. Both histograms peak at V = 0 ensuring that there is no systematic error in the flux-density measurements. The

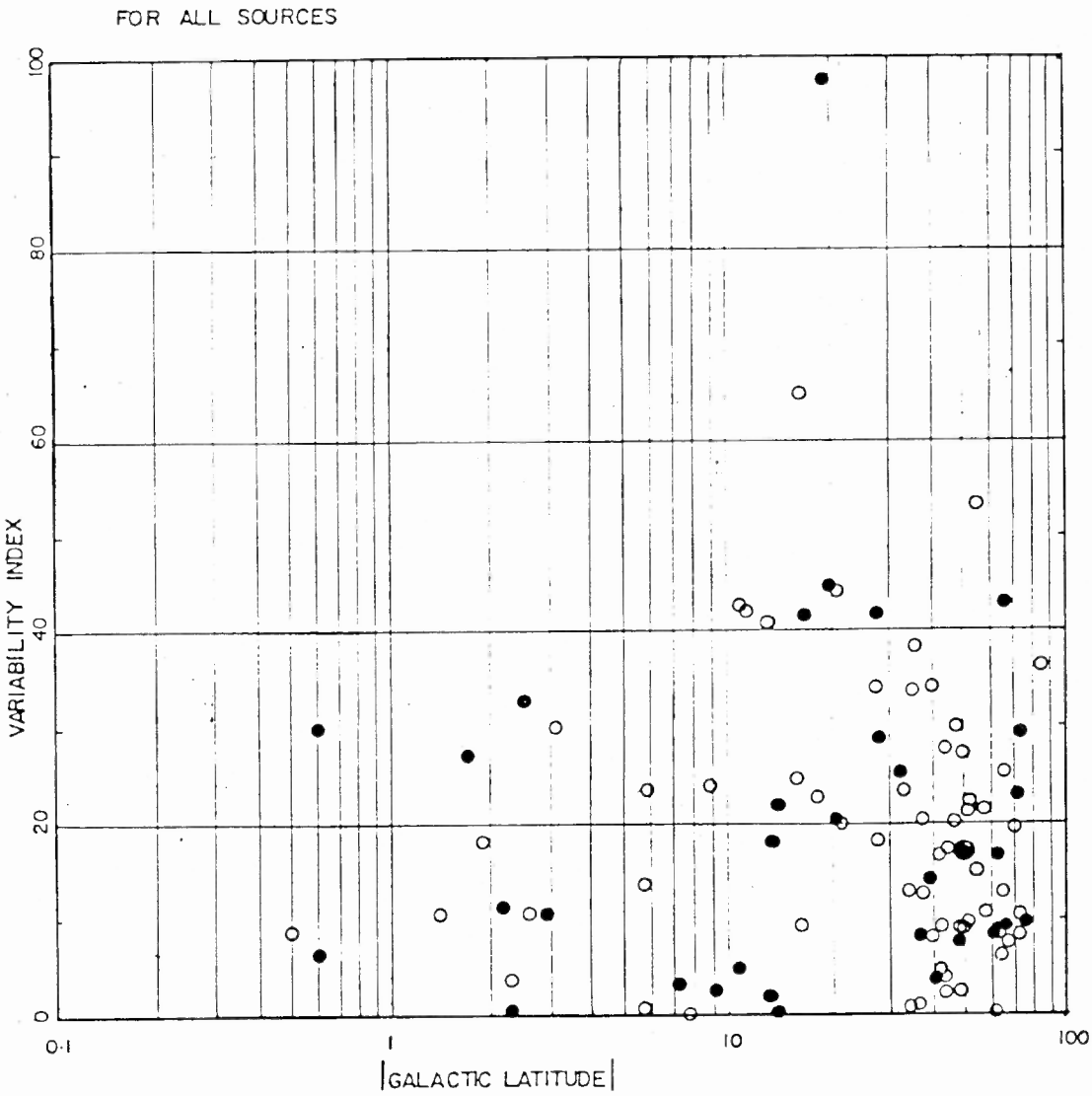

Fig. V-2: The modules of variability index for each source as a function of the absolute value of its galactic latitudes.

Gaussian fitted to histogram 'A' has a standard deviation, σ = 5 %, while for B, σ = 25 %. We conclude that flux-density variations down to 15 % can be believed at the 3σ level.

In Fig. V-2 we have plotted the modulus of the variability indices (V) for all the compact sources as a function of galactic latitude. A filled circle represents an increase in the flux density between the two epochs, while an open circle denotes a decrease. The large scatter in this plot can be attributed mainly to the two-point sampling function, i.e. the expected difference of variability time-scales with latitude and that the sources have been observed just at two epochs separated by ~ 14 yr. In a recent study of the effect of short data stretchs on the estimation of intensity fluctuations, Deshpande and Nityananda (1990) have used Monte-Carlo simulations to generate various realisations of S(t), the flux density as a function of time, on the basis of the equivalent thin-screen RISS model of Blandford and Narayan (1985). From these simulated data, they have calculated the apparent modulation index, m_a which is related to the first-order structure function of intensity fluctuations as:

$$m_a(t_{obs}) = \sqrt{\{ D_I(t_{obs}) \}} \qquad \text{-----(5.5.2)}$$

where, $D_I(t_{obs})$ = the structure function

$$= \frac{1}{\bar{S}^2} \{ S(t) - S(t+t_{obs}) \}^2 \qquad \text{------(5.5.3)}$$

However, in the definition of structure function, $\bar{S}^2$ should be the true mean value of the flux density, a condition which, as they point out is not met for a limited-data stretch. In Fig. V-3a we reproduce their plot of $m_a(t_{obs})/m_\infty$ (where, m_∞ is the asymptotic value) and its variance

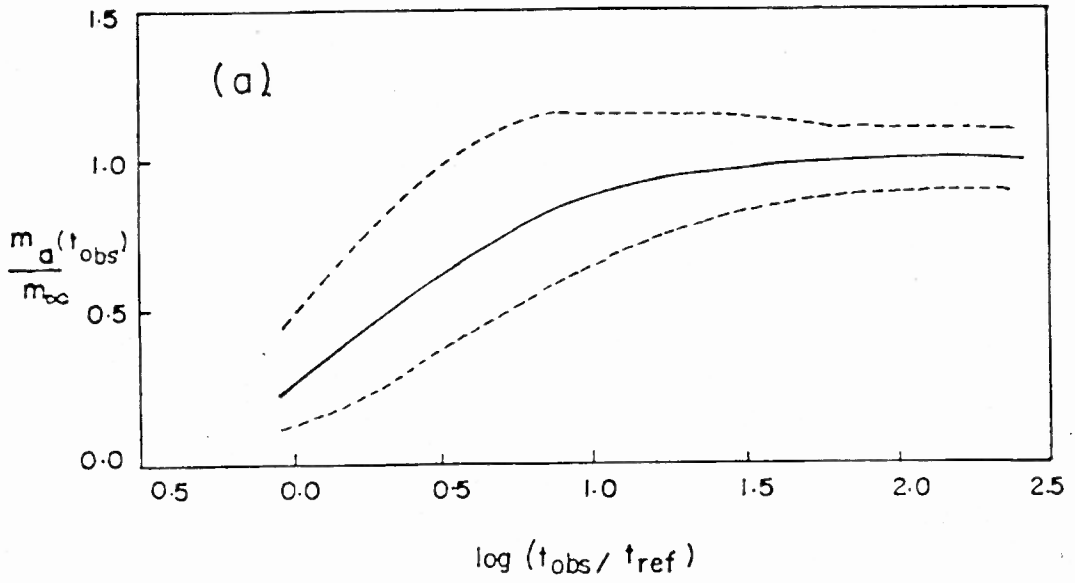

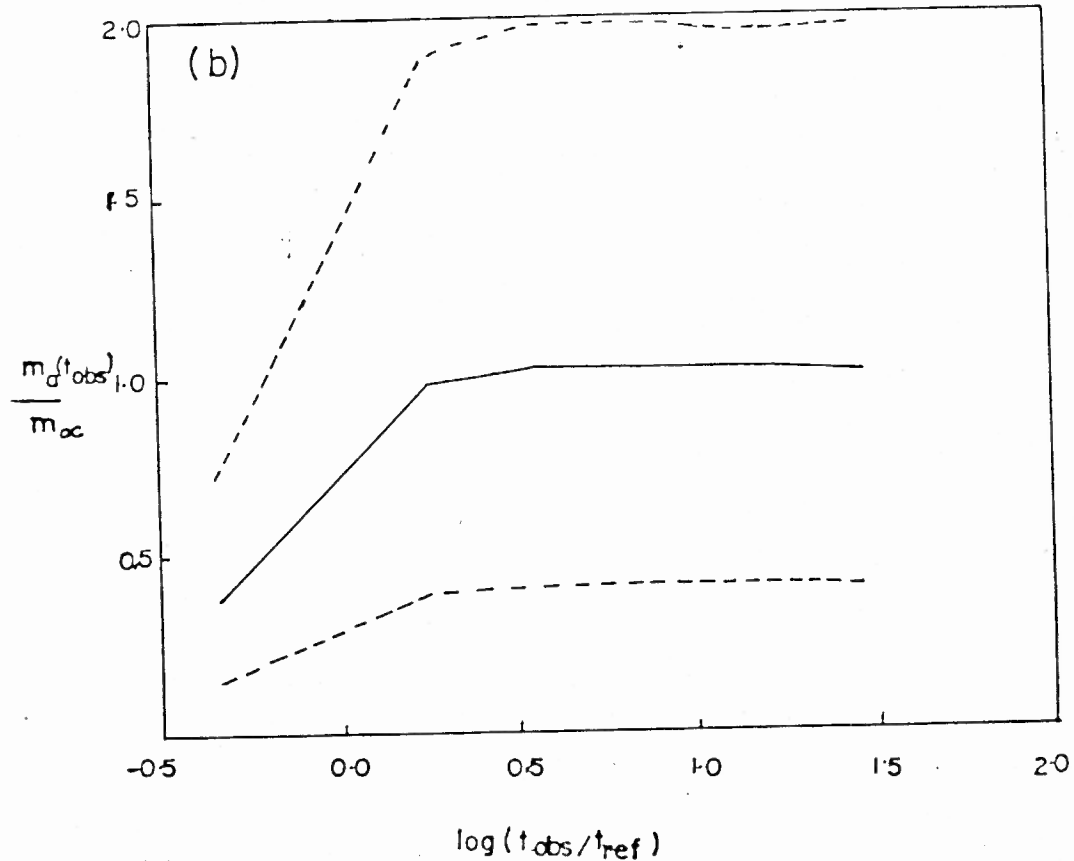

Fig. V-3: (a) Apparent modulation index over a particular observing time (t_{obs}) as a function of the ratio of the observing time and the refractive time scale (reproduced from Deshpande & Nityananda, 1990).

(b) Similar plot for a two-point sampling function.

(derived from their many trials) against t_{obs}/t_{ref}, the ratio of the observing time-span (t_{obs}) and the refractive time-scale (t_{ref}). Fig. V-3b shows a similar plot to Fig. V-3a calculated using the same algorithm but for the case of a two-point sampling function. The variance in this case is ~100% in contrast with the moderate value of ~ 30% in Fig. V-3a. This is reflected by the large scatter of the variability indices seen in Fig. V-2 for sources within any particular latitude bin.

The distribution of variability indices within a particular latitude bin can be considered to be a zero-mean Gaussian. The standard deviation of this distribution is a parameter which is analogous to the modulation index, m, defined as the rms of the 'light-curve' divided by its mean for a hypothetical source at the mean bin-latitude (assuming that ergodicity is valid here, so that the time-series of the percentage flux-density deviations from the mean of the hypothetical source can be replaced by the ensemble derived from the two-point variability indices, V, of a number of sources). We designate this quantity by m_e and calculate its value for each latitude bin using:

$$m_e = \sqrt{\{ m_e'^2 - \varepsilon_v^2 \}} \qquad \text{------(5.5.4)}$$

$$\text{where, } m_e' = \sqrt{\left\{ \frac{\sum_{i=1}^{N} V_i^2}{N} \right\}} \qquad \text{-----(5.5.5)}$$

$$\text{and } \varepsilon_v = \sqrt{\{(\%\text{ error in } S_1)^2 + (\%\text{ error in } S_2)^2 \}} \qquad \text{----(5.5.6)}$$

$$= 8.6\ \%\ \text{ at high latitudes } (|b| > 3^\circ)$$

$$= 11.2\ \%\ \text{ at low latitudes } (|b| < 3^\circ)$$

The error in m_e is calculated using:

$$\sigma(m_e) = \frac{m_e'}{\sqrt{2N}} \qquad \text{-----(5.5.7)}$$

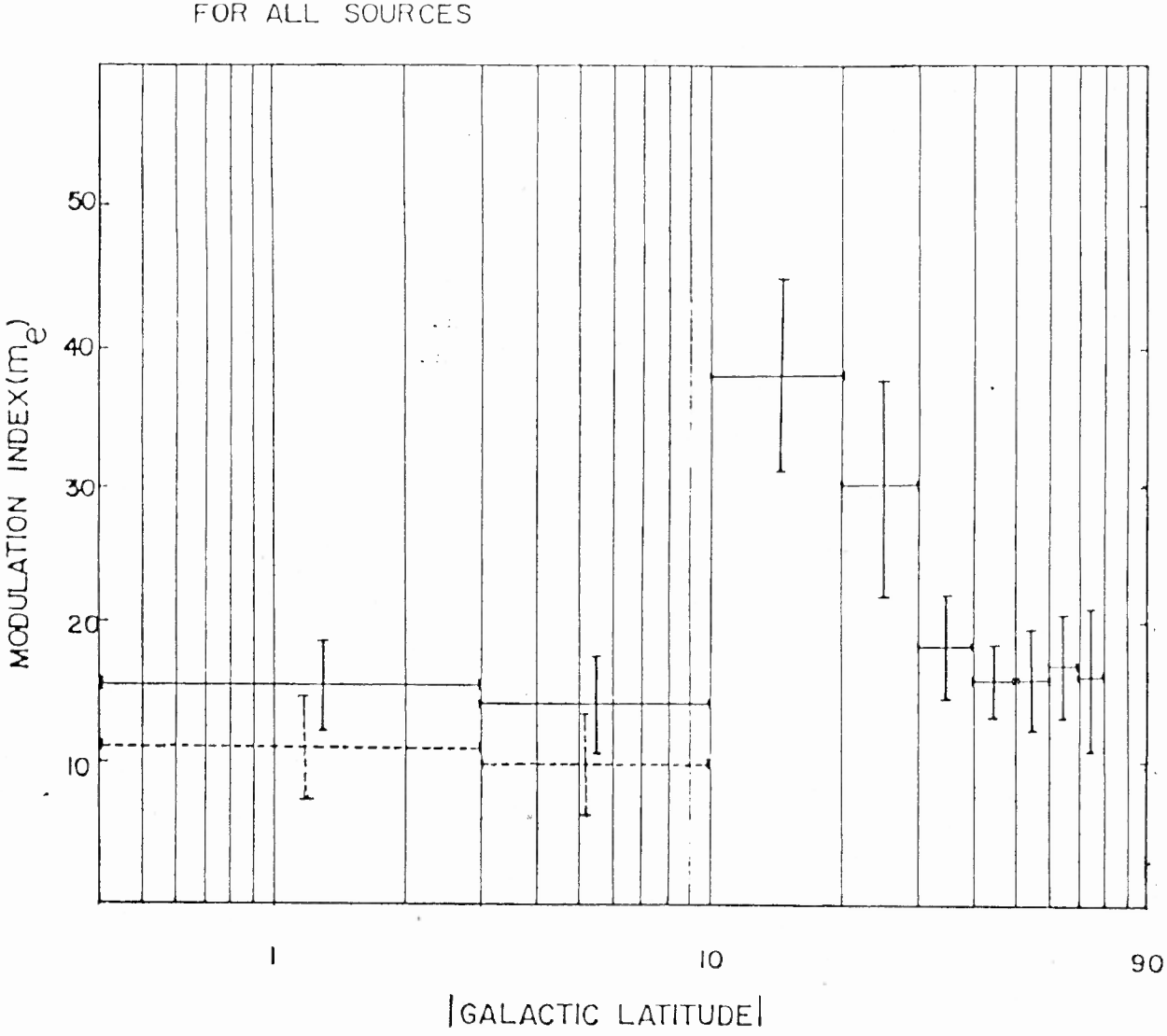

Fig. V-4: Modulation indices at different latitude bins.

In Fig. V-4 we have plotted these modulation indices (m_e) and their errors for the total sample divided between the indicated latitude bins. At low latitudes ($|b|<10°$), the refractive timescales at metre wavelengths are expected to be much longer than the time span of the Molonglo survey. Hence for low-latitude sources, S_1 is not a proper estimate of the true-mean value of the flux densities. The standard deviation of variability indices (V) for low-latitude bins are therefore higher than the true modulation index by a factor of $\sqrt{2}$. We have incorporated this correction for the latitude-bins below 10° and the corrected m_e values are marked by dotted lines.

The main features of Fig. V-4 are:

1. The modulation index is comparatively low for sources situated at low galactic latitudes ($|b| < 5°$).

2. There is a sudden rise in variability to a peak at $|b| \sim 15°$.

3. At higher latitudes the modulation index falls-off and reaches almost a constant value for $|b| \geq 45°$.

In order to test the statistical significance of these trends, we have calculated the Cramer-Coefficient (Siegal and Castellan, 1988) using a 2 × 4 contingency table (Table V-5). Since this test can be applied only to a nominal data-set, we have counted the numbers of variable ($|V| > 20\%$, a more conservative definition than in Table V-1) and nonvariable sources in four latitude intervals, chosen such that roughly equal numbers of sources fall within each bin. However, this is not a prerequisite for this test. The C-coefficient used in this test is defined as:

TABLE V-5: 2 X 4 CONTINGENCY TABLE

LATITUDE RANGE	VARIABLES n_{ij}/E_{ij}	NONVARIABLES n_{ij}/E_{ij}	R_i
0 - 10	7/8.75	13/11.26	20
10 - 30	16/9.63	6/12.38	22
30 - 50	10/12.69	19/16.31	29
50 - 90	9/10.94	16/14.06	25
C_j =	42	54	

$$C = \sqrt{\left\{ \frac{\chi^2}{N\,(L-1)} \right\}} \qquad \text{------(5.5.8)}$$

where, N is the total no. of sources

and L is the minimum of the nos. of rows and columns in the contingency table (L = 2 in the present case).

χ^2 is calculated using the relation:

$$\chi^2 = \sum_{i=1}^{r} \sum_{j=1}^{k} (n_{ij} - E_{ij})^2 / E_{ij} \qquad \text{------(5.5.9)}$$

where n_{ij} is the no. in the i-jth entry in the r × k contingency table

and E_{ij} is the expected value of n_{ij} in the case where there is no dependence between the row and column parameters. It is calculated using the relation:

$$E_{ij} = \frac{R_i C_j}{N} \qquad \text{------(5.5.10)}$$

where, $$R_i = \sum_{j=1}^{k} n_{ij}$$

and $$C_j = \sum_{i=1}^{r} n_{ij}$$

The value of the C-coefficient is zero for no dependence and unity for a one-to-one correspondence between the row and the column parameters. In the present case we obtain a value of C ~ 0.33 which shows that there is a dependence of LFV on galactic latitude. The statistical significance of this dependence can be estimated by finding the probability of the null hypothesis, $p(H_0)$, this hypothesis being that there is actually no association between the two parameters and the observed effect is just an artifact of a chance coincidence. This is achieved using the χ^2 value for

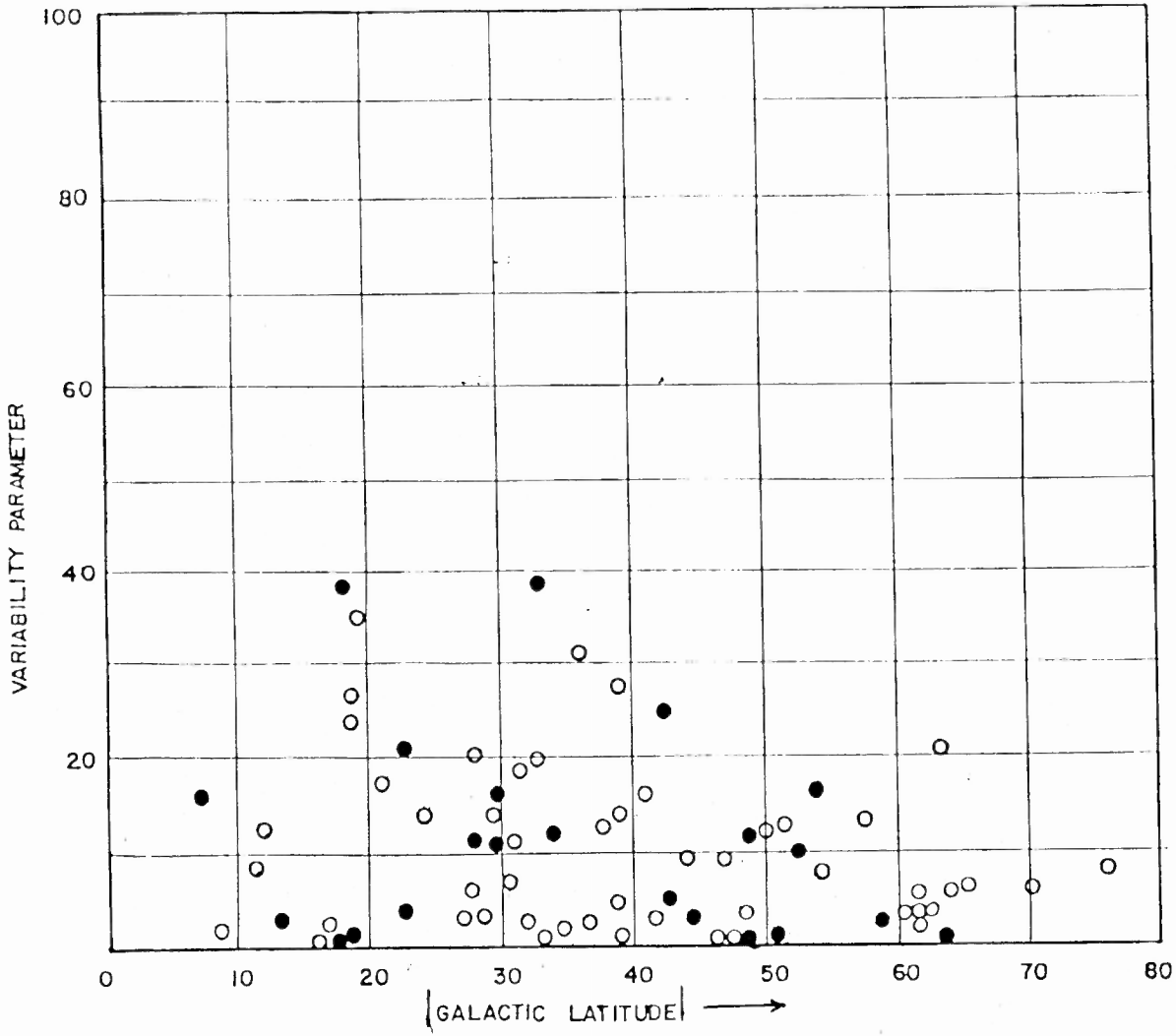

Fig. V-5: The percentage variability parameter of the sources with Flat and unknown spectra from Condon et al. (1979) against the galactic latitudes.

a frequency, df = 2 in this case. We find that

$$p(H_0) = 0.02 \qquad \text{------(5.5.11)}$$

Hence, it can be concluded that the observed trend is statistically significant at the 98 % confidence level.

We have looked for evidence of similar effects in the LFV monitoring programme of Condon et al. (1979) since they have also used 2-point sampling over a similar time-interval. However, the distribution of sources was not uniform over galactic latitude for this sample and in particular, low galactic latitudes were avoided. In Figs. V-5 we have plotted their variability parameters against $|b|$. The maximum variability seems also to occur at intermediate latitudes ($|b| \sim 20°$).

Further, we have divided all our sources into two subclasses covering the longitude ranges of $270° < \ell < 90°$ (towards the galactic centre) and $90° < \ell < 270°$ (anticentre). In Figs. V-6a and b, the modulation indices over the indicated bins of galactic latitudes for the galactic-centre and the anticentre subgroups are plotted against $|b|$, along with the individual values of V. Both the subgroups show very similar trends to those mentioned above for the combined sample (Fig. V-4). However, it appears from Fig. V-6 that when compared with the galactic-centre subsample, the anticentre subsample shows a steeper/narrower peak at a lower latitude.

In order to determine the statistical significance of any differences between the centre and anticentre samples in the presence of the large error-bars (Figs. V-6a and b) we have employed a χ^2-test. The value of χ^2 has been calculated by:

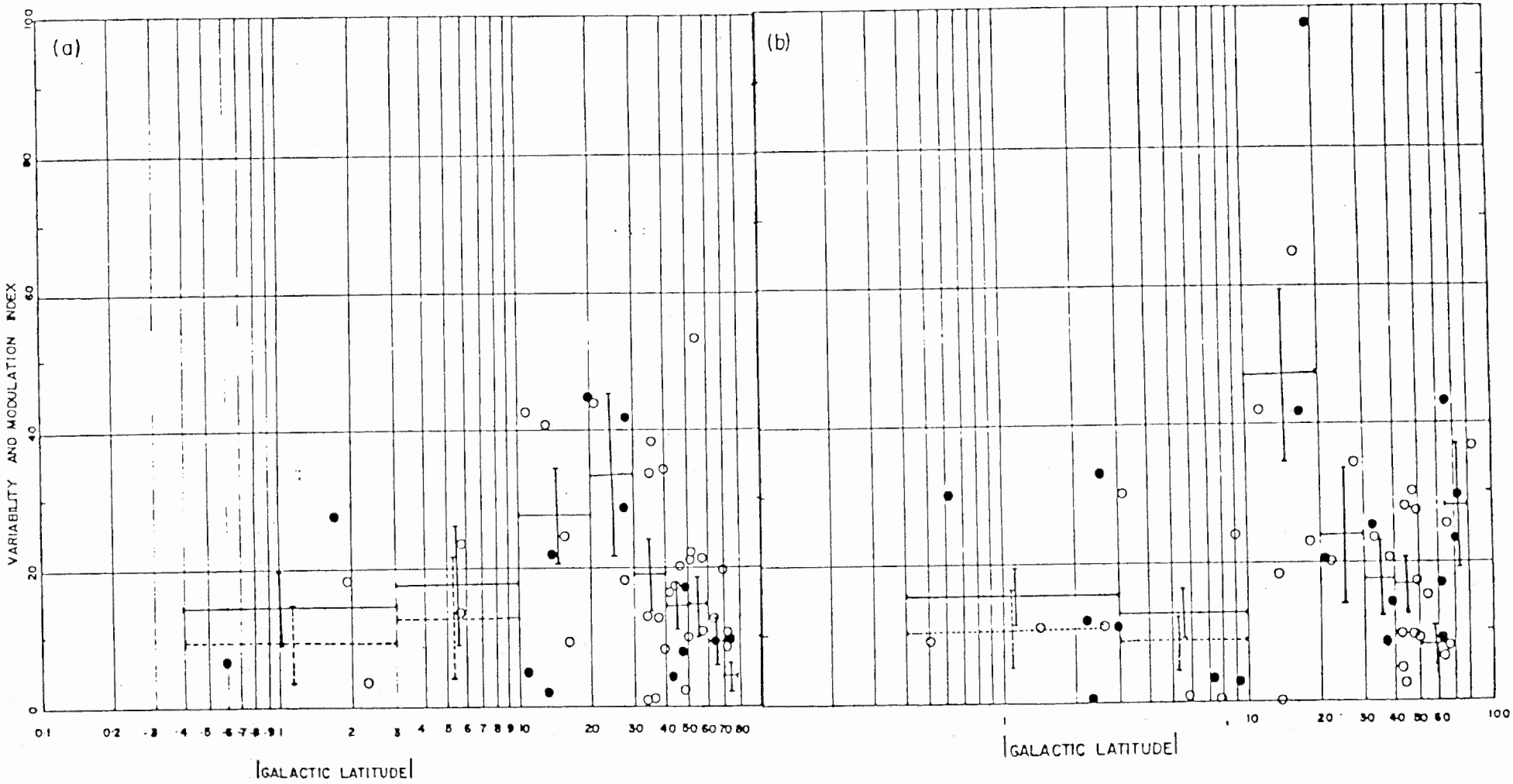

Fig. V-6: Latitude dependence of variability and modulation indexes for the galactic-centre (a) and the anticentre (b) subsample.

$$\chi^2 = \sum_{i=1}^{7} \left\{ \frac{m_e(GC)_i - m_e(AC)_i}{\sqrt{[\sigma_{m_e(GC)i}{}^2 + \sigma_{m_e(AC)i}{}^2]}} \right\}^2 \qquad \text{-----(5.5.12)}$$

We have excluded the last two bins as their sizes differed for the two samples in order to accomodate at least five sources within each bin. The value of χ^2 is found to be 4.36 which suggests that for a frequency, df = 6, the probability of the two samples being drawn from the same population is ~ 50 %. Hence, we conclude that our data do not show a significant difference in the nature of the latitude dependence of variability between the galactic-centre and anticentre directions.

5.6 DISCUSSION

At high latitudes ($|b| > 30°$), since the refractive time-scales are of the order of a few months, a saturated value of the modulation index (m) of ~ 0.5 is expected over a time interval of 14 yr which should also be latitude independent. The observed fall in m_e at high latitudes can be explained only if the intrinsic sizes of the compact sources are larger than the interstellar scattering angles for these lines-of-sight. The observed modulation index will then be reduced by a factor $(\theta_{scat}/\theta_{int})$ and will have a slow latitude dependence via the scattering angle. Due to large error bars, no latitude dependence is discernable above a latitude of 40°.

The low value of modulation index at low galactic latitudes in the galactic-centre quadrant is perhaps a manifestation of very large scattering along such lines-of-sight which causes the time-scales for RISS (t_{ref}) to be very long compared to the observing time-interval (t_{obs}). Hence, only a fraction, $(t_{obs}/t_{ref})^n$ (Chapter II) of the true modulation index will be observed, even for a point source. There is ample observational evidence for such an enhanced-scattering region in the inner

Galaxy (Rao and Ananthakrishnan, 1984; Dennison et al., 1984). However, in the anticentre quadrant, the lines-of-sight are not likely to pass through this region. Therefore, the low modulation index for $\ell \sim 180°$, $|b| \leq 10°$ is rather unexpected. If the distribution of the electron-density fluctuations or the scattering strength, C_N^2 in the Galaxy were known, one could predict the modulation index for any line-of-sight. The inverse problem is much less straight-forward since there are other unknown factors, e.g. the intrinsic size of the source, the fraction of the total flux density in the compact component, any residual intrinsic variability, short and inadequately sampled data stretches, etc. In fact, because of the noise-like nature of these intensity variations, it is very difficult to define a proper sampling interval. This led us to compare the latitude dependence of variability with the predictions from a number of models. Using additional information from angular-broadening measurements along various lines-of-sight, we have tried to eliminate some of the models investigated. However, we stress that this does not ensure the uniqueness of the model that fits our data best.

Model fitting:

For a particular distribution of scattering strength, $C_N^2(s)$ we have calculated the angular broadening due to diffractive interstellar scattering using the relation (Rao and Ananthakrishnan, 1984):

$$\theta_{scat}(\text{mas}) = 17.2 \times (\lambda_m)^{2.2} \left[\int_0^S C_N^2(s')\, ds'\right]^{0.6} \qquad \text{-----(5.6.1)}$$

where, λ_m is the observing wavelength in metres and s' is the distance along the line-of-sight in parsec. The power-spectrum of the electron-density irregularities is assumed to be of a Kolmogorov nature.

Further, we have assumed that the angular broadening is due to an

equivalent thin-screen at a distance s_{eq} from the observer, where,

$$s_{eq} = \sqrt{\left\{ \frac{\int_0^S s'^2 \, C_N^2(s') \, ds'}{\int_0^S C_N^2(s') \, ds'} \right\}} \qquad \text{-----(5.6.2)}$$

For a particular assumed intrinsic size (θ_{int}) the variability time-scale is then

$$t_{ref} = \frac{s_{eq} \times \theta}{V_{rel}} \qquad \text{-----(5.6.3)}$$

where, $\theta = \theta_{scat}$, for $\theta_{scat} > \theta_{int}$

$= \theta_{int}$, for $\theta_{scat} < \theta_{int}$

and V_{rel} = the projected relative velocity between the equivalent screen an the observer. This was taken to be 100 km s^{-1} (Rickett, 1986).

The expected modulation index is (Chapter II):

$$m = 0.5 \times \tau \times \delta \qquad \text{-----(5.6.4)}$$

where, $\tau = t_{obs}/t_{ref}$ for an observing time-interval, $t_{obs} < 0.7 \times t_{ref}$

$= 1$ otherwise

and $\delta = \theta_{scat} / \theta_{int}$, for $\theta_{scat} < \theta_{int}$

$= 1$ otherwise.

In all our calculations, we have used t_{obs} = 16 yr for $|b| < 3°$ and 14 yr for higher latitudes as the interval between the two epochs of observation and a value of 15 mas for the intrinsic size, θ_{int}.

In addition to the observed latitude-dependence of variability (Figs. V-6a and b), the following observed values for the 327-MHz interstellar scattering angles have been used as constraints for the models considered here:

(a) θ_{scat} ($|b|=90°$) $\leq$ 7 mas (Duffet-Smith and Readhead, 1976)

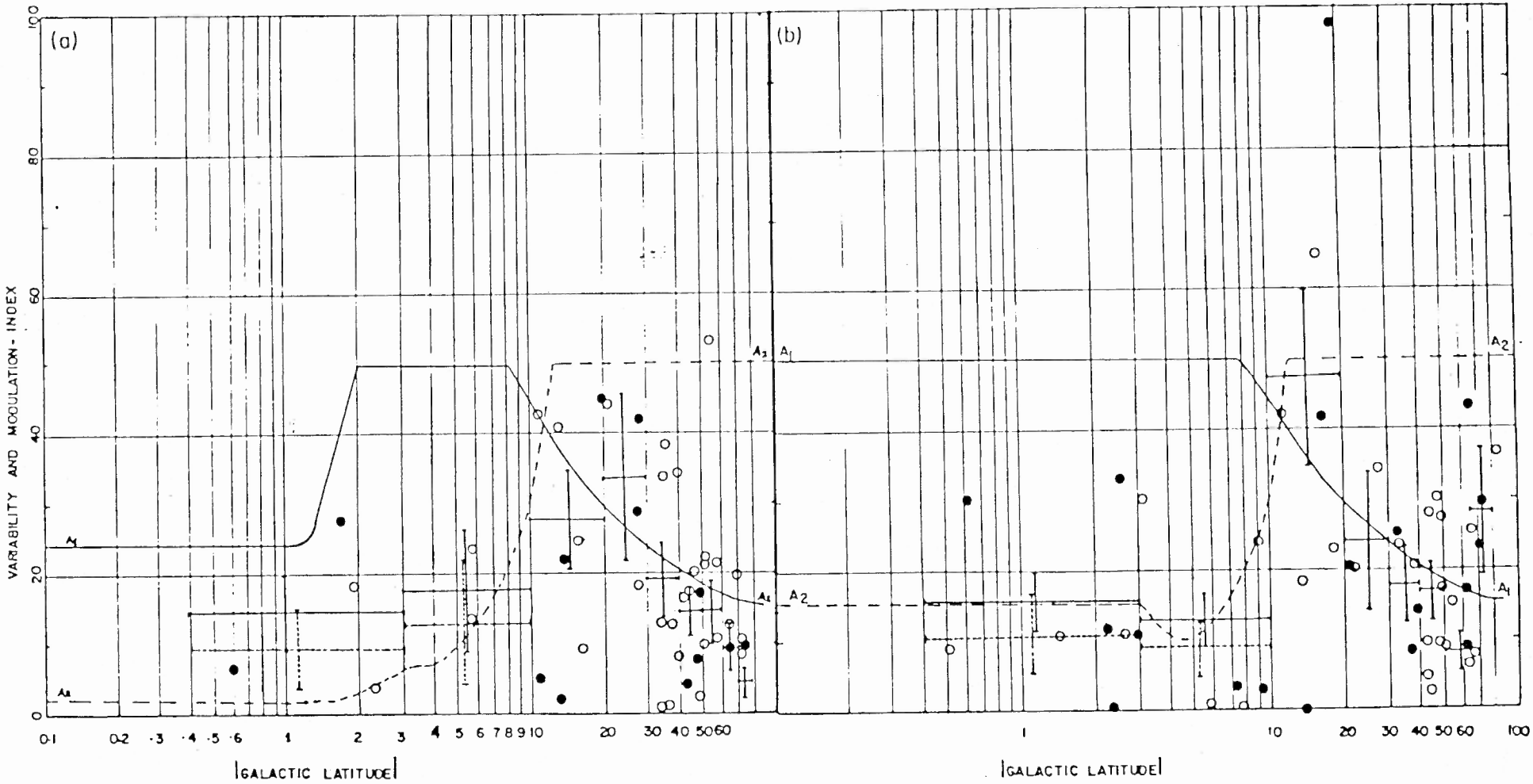

Fig. V-7 : Predict d modulation indixes from model A1 and A2 for the galactic centre (a) and the anti-centre (b) direction.

(b) $\theta_{scat}(\ell=180°, b=0°) \leq 200$ mas (Rao and Ananthakrishnan, 1984)

(c) $\theta_{scat}(\ell=4°, b=0°) \approx 1.4$ arcsec (Chapter VI)

For all models, we have assumed that the Sun is located in the plane of the Galaxy, at a radial distance of 8.5 kpc from the galactic centre. We have neglected any possible clumping of the scattering material.

Model A1:

There is some evidence from studies of the scatter-broadening of extragalactic radio sources and the diffractive ISS of pulsars that the C_N^2 distribution can be described by a two-component model (Rao and Ananthakrishnan, 1984; Dennison et al., 1984; Cordes, Weisberg and Boriakoff, 1985). The first component is a disk of ± 500 pc thickness with a galactocentric-distance-independent value of scattering strength, $C_N^2 \approx 10^{-3.5}\ m^{-6.67}$. The second component is a thinner region of enhanced scattering in the inner Galaxy, whose scattering strength decreases with increasing galactocentric distance.

In the anticentre direction, the line-of-sight is not expected to pass through the second component, even at very low latitudes. Hence, in our first model (A1) we have used only the extended component to calculate the expected modulation index as a function of latitude in the anticentre direction.

The functional form used for C_N^2 as a function of galactocentric distance, r and height above the galactic plane, z is:

$$C_N^2(r,z) = C_N^2(0)\ \exp[-|z|/Z_o] \qquad \text{------(5.6.5)}$$

where, $C_N^2(0) = 10^{-3.5}\ m^{-6.67}$ for $r \leq 15$ kpc

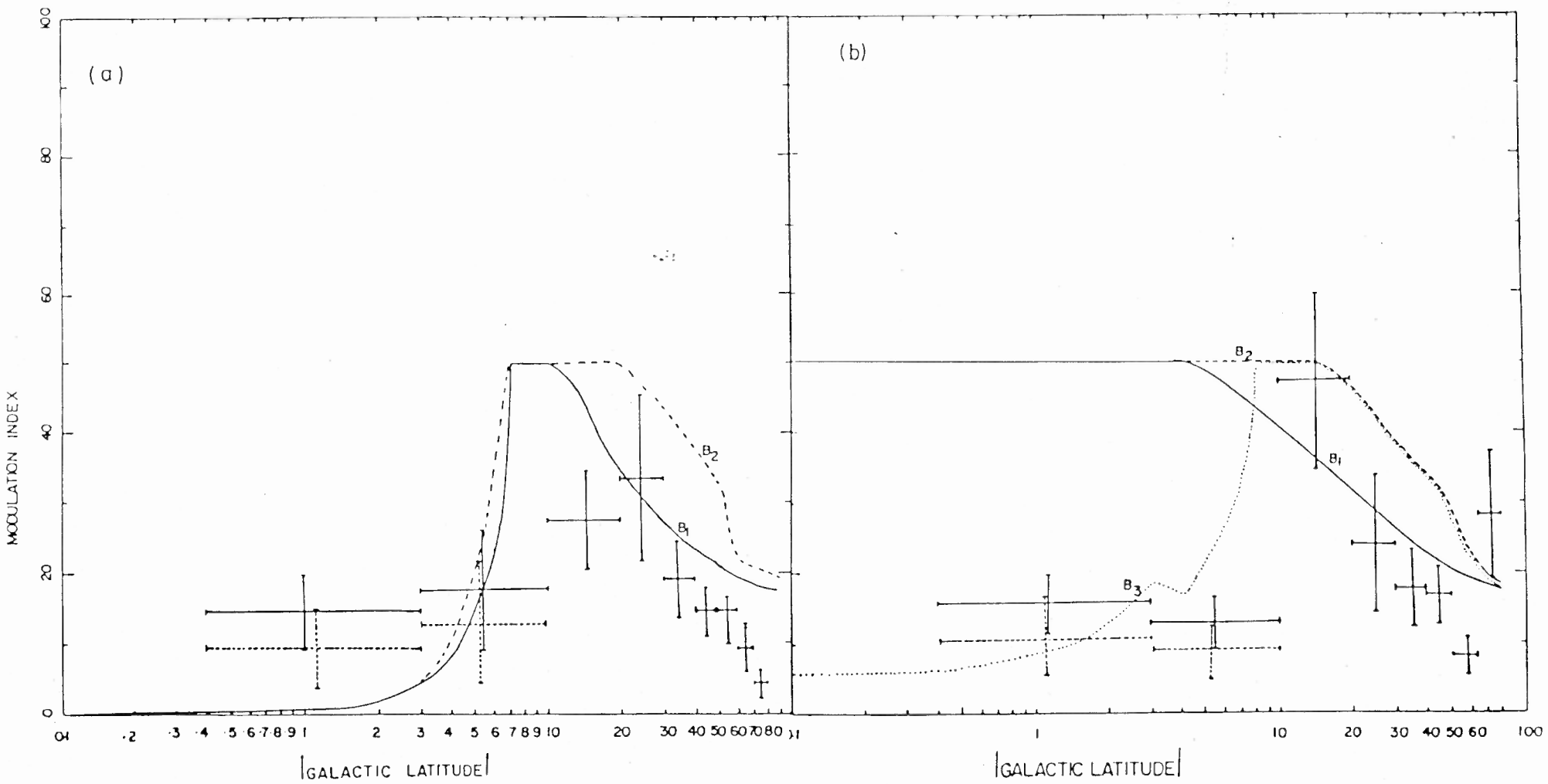

Fig. V-8: Predicted modulation indices from models B1, B2 and B3; functions of latitude for the galactic-centre (a) and the anticentre (b) directions.

$= 0$ otherwise

and $Z_o = 0.5$ kpc

The resulting curve (A1) is superposed on the observed m_e vs $|b|$ plot in Figs. V-7a and b. For high latitudes, it agrees well with the observations, predicting the value of $\theta_{scat}(|b|=90°)$ to be 5.4 mas. However, the fit fails completely at low latitudes ($|b| < 10°$) in the anticentre direction (Fig. V-7b).

Model A2:

In order to obtain better agreement between the predictions of the model and the observations, we have next varied the parameters $C_N^2(0)$ and Z_o. The best fit at low-latitudes for the anticentre direction (curve A2 in Fig. V-7b) is obtained for the following values of the parameters:

$$C_N^2(0) = 10^{-2} \; m^{-6.67}$$

$$Z_o = 0.65 \text{ kpc}$$

However, this gives a value of $\theta_{scat}(|b|=90°) = 64$ mas. Hence, even for the anticentre direction the single-component model is inadequate to explain the observed effects.

Model B:

From the observed deficiency of compact sources showing interplanetary scintillations (IPS) at low galactic latitudes in the galactic-centre quadrant, Rao and Ananthakrishnan (1984) have proposed analytical expressions for the enhanced scattering region in the inner Galaxy. We have tried to fit the present data with models having the linear and exponential radial dependencies that they suggest. The C_N^2 distributions in these two cases are taken to be

$$C_N^2(r,z) = C_{N1}^2 \exp[-(|z|/Z_1)] + C_{N2}^2 f(r) \exp[-(z/Z_2)^2] \quad ---(5.6.6)$$

The first term describes the extended component as used in A1 and the second

term expresses the r,z-dependence of the enhanced scattering region. The function, f(r) for the models of Rao and Ananthakrishnan are:

(1): $f(r) = 1 - r/R_2$ for $r < R_2$

$= 0$ otherwise.

(2): $f(r) = \exp(-r/R_2)$

We have used the best-fit parameters of Rao and Ananthakrishnan for the second component (scaled for a solar galactocentric distance of 8.5 kpc) while retaining the same parameters for the first component as in A1.

Parameter values:

Model	C^2_{N1}	R_2(kpc)	Z_2(kpc)
B1: linearly-decreasing	8.3	6	0.075
B2: exponential	56.7	0.85	0.075

The curves B1 and B2 in Figs. V-8a and b are the corresponding latitude-dependencies of variability in the centre and anticentre directions. While for the galactic-centre direction both B1 and B2 agree quite well with the observations, at low-latitudes in the anticentre direction they deviate widely from the observations. In order to generate a better fit to the low-latitude anticentre behaviour, it is necessary to assume that the enhanced scattering region extends beyond the solar circle. The curve B3 in Fig. V-7b is generated for a linearly-decreasing r-dependence, as in model B1 but with R_1 taken to be 15 kpc. Although such a model can predict the observed low-latitude anticentre behaviour, it also predicts a large scattering angle at the pole. This is

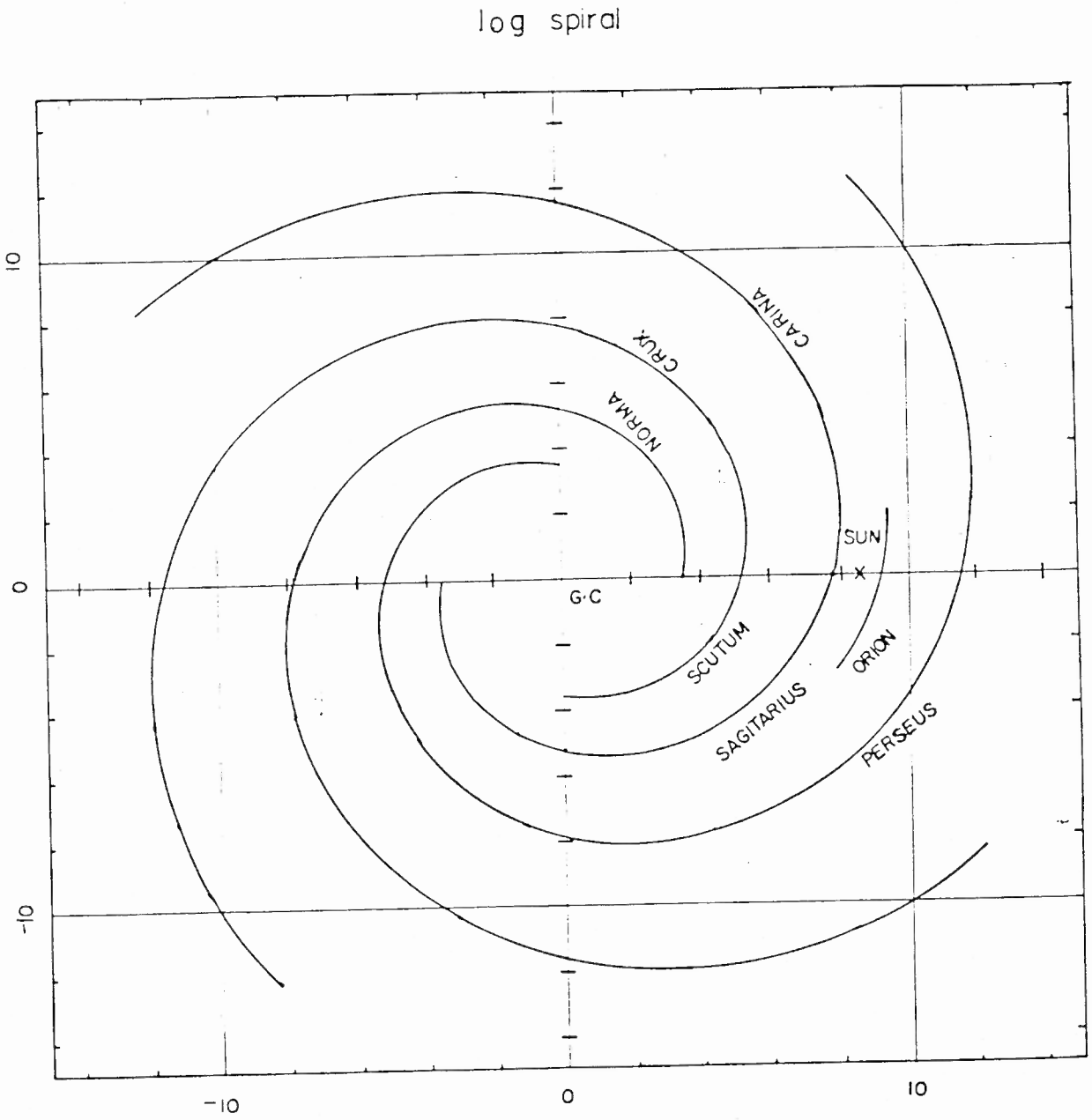

Fig. V-9: Schematic diagram of the spiral structure showing the locations of various arms. Both the axes represent galactocentric distances in kpc. This has been used in models C1 and C2.

demonstrated in Fig. V-11, where curve B3 shows the scatter-broadening in the anticentre direction as a function of latitude for this model.

The above exercise made it clear that if such a model were to generate the observed latitude dependence of variability, it would have to be assumed that in model B3 the Sun is located in some sort of a 'local hole' such that the high-latitude lines-of-sight experience only low scattering. One plausible model that is compatible with such a situation is to assume a spiral nature for the electron-density distribution with the Sun located within an inter-arm region.

Model C (The spiral model):

We have investigated a 4-arm logarithmic spiral distribution with a pitch angle of $14^{o}.25$, which resembles the spiral model of the Galaxy suggested by Georgelin and Georgelin (1976), with the addition of an 'Orion' arm-segment (Fig. V-10). The functional form of the C_N^2 distribution assumed for this model Galaxy is:

$$C_N^2(r,z) = \sum_{i=1}^{NS} C_{NS}^2 \exp\left[-\left(\frac{R_{si}-r}{W_{si}}\right)^2\right] f(r)\, f(z) + C_{NI}^2 \exp\left[-\left(|z|/Z_I\right)\right] \text{ for } r < 15 \text{ kpc}$$

$$= 0 \text{ , otherwise} \qquad \text{-----(5.6.7)}$$

Here, the first term expresses the contribution from each of the spiral arm crossings (NS in number) that a particular line-of-sight makes. Because of the Gaussian function, at a particular point only the nearest spiral arm makes any significant contribution). The second term represents the low-scattering, extended component (the same as the first component of models A1 and B). The value of C_{NS}^2, the measure of the scattering strength on the axis of the spiral arm, is independent of galactocentric radius, while the radial distribution within an arm is assumed to be Gaussian of width W_{si}. R_{si} is the galactocentric distance

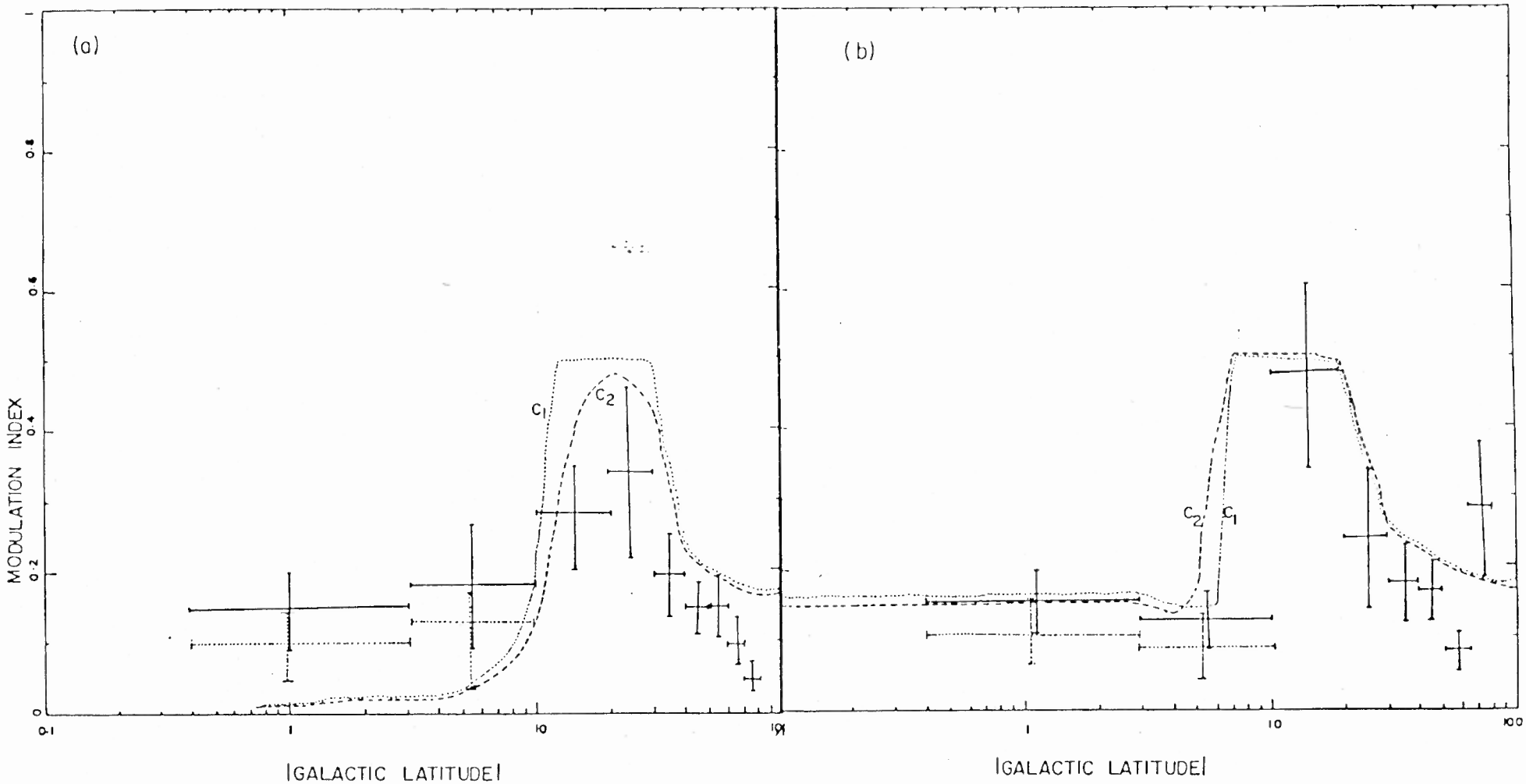

Fig. V-10: Predicted modulation indices from models C1 and C2 for the galactic centre (a) and the anticentre (b) directions.

at which the line-of-sight intersects an arm, while the arm extends up to a height of Z_{s2} perpendicular to the plane of the Galaxy. Also,

$$f(r) = 1, \text{ for } r < 15 \text{ kpc}$$
$$= 0, \text{ for } r > 15 \text{ kpc}$$

and

$$f(z) = \exp[-(|z|/Z_{s1})], \text{ for } z < Z_{s2}$$
$$= 0, \text{ otherwise}$$

Figs. V-10a and b show the calculated latitude dependence of the modulation index for the galactic-centre and anticentre directions (C1). The best-fit values of the parameters are:

For the extended/inter-arm component:

$$C_{NI}^2 = 0.0002\ m^{-6.67}$$
$$Z_I = 1 \text{ kpc}$$

For the spiral component:

$$C_{NS}^2 = 0.75\ m^{-6.67}$$
$$W_{si} = 200 \text{ pc}$$
$$Z_{s1} = 1.5 \text{ kpc}$$
$$Z_{s2} = 300 \text{ pc}$$

In order to take account of the fact that our observed sources are distributed over a range of longitudes for each subsample, we have calculated the average modulation index as a function of latitude for the following longitude ranges:

(i) $-10^\circ \leq \ell \leq 40^\circ$

(ii) $170^\circ \leq \ell \leq 220^\circ$

The curve C2 in Figs. V-10a and b show the results for these averaged

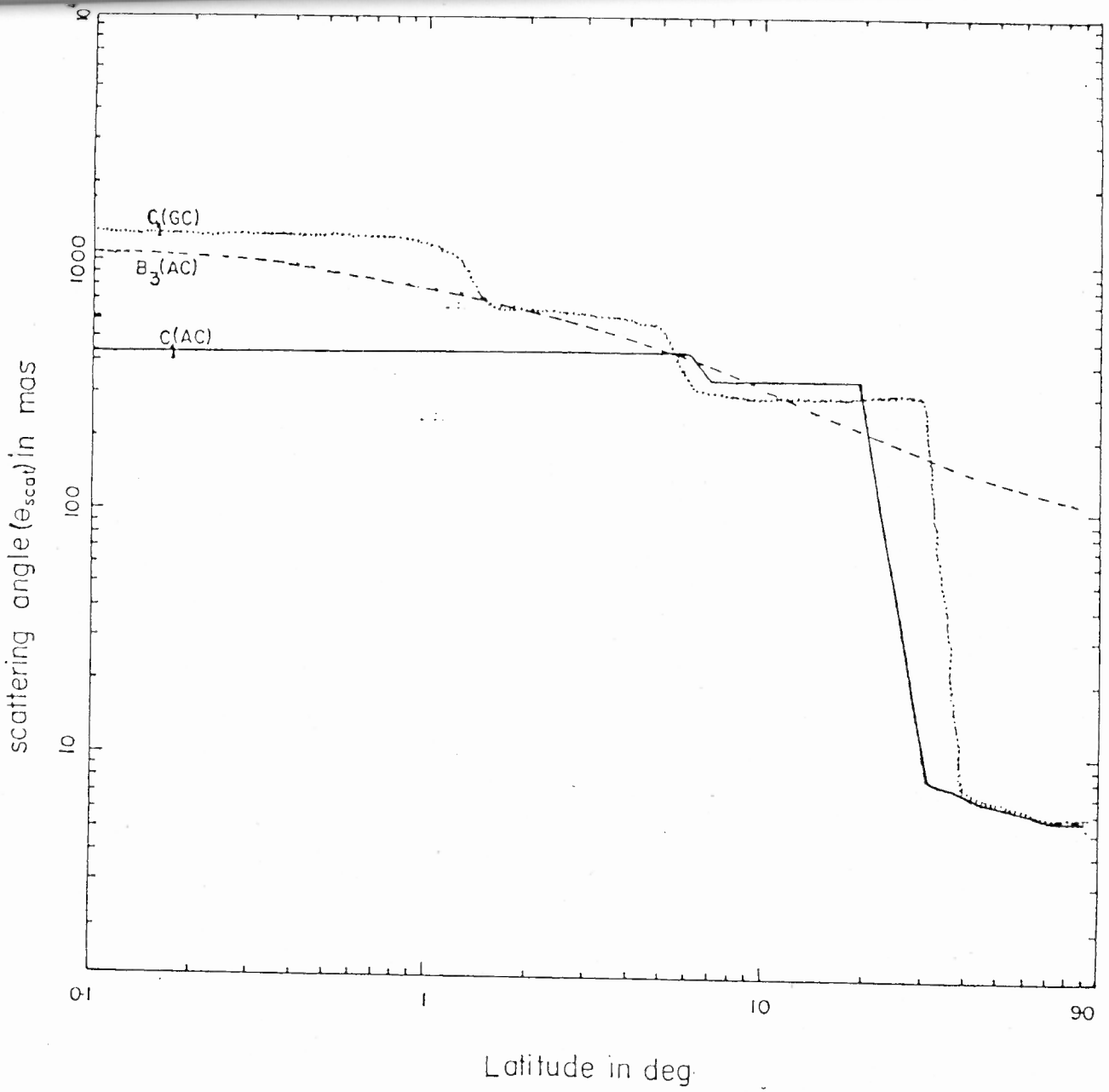

Fig. V-11: The predicted scattering angles from the models B3 and C1 (see text) as functions of galactic latitude for the galactic centre (GC) and anticentre (AC) directions.

modulation indices. The agreement with the observations is fairly good. The merit of this model is that it can predict the general form of the observed latitude dependencies for both the galactic-centre and anticentre quadrants for a single set of parameter values. However, the low-latitude value of θ_{scat} for the anticentre direction (see Fig. V-8) is a factor of ~ 2 higher than the value of ~ 200 mas inferred from the IPS observations (Rao and Ananthakrishnan, 1984). One possible explanation is that, due to its proximity to the Sun, the Orion arm is less effective than the Perseus arm in causing RISS. In this case, it would still be possible to generate low modulation indices for the low-latitude, anticentre directions, as the distance to the equivalent thin screen would be much larger causing longer refractive time-scales of variability but with a much smaller value of θ_{scat} in the plane (~ 150 mas).

If this spiral model is indeed a better description of the true C_N^2 distribution, then it should be possible to identify its effects in other observations of interstellar scintillations. Especially, it would be worthwhile to investigate whether the noted large scatter in the value of C_N^2 (by about 4 orders of magnitudes) from pulsar-observations (Cordes, Weisberg and Boriakoff, 1985) could be explained by invoking a spiral distribution of turbulence.

One observational test for this model would be to look for regions of high and low scatter-broadening at various longitudes for low-latitude lines-of-sight and to see if these coincide with spiral-arm and inter-arm regions respectively.